# PERFORMANCE MAP OF RADIAL FANS THROUGH CFD TECHNIQUES

**Ramiro G. Ramirez Camacho**
Universidade Federal de Itajubá
Campus Prof. Jose Rodrigues Seabra - Av. BPS nº1303, Bairro Pinheirinho Cep 37500-903 Itajubá MG -Brasil
rgramirez65@hotmail.com

**André Makishi**
Universidade Federal de Itajubá
Campus Prof. Jose Rodrigues Seabra - Av. BPS nº1303, Bairro Pinheirinho Cep 37500-903 Itajubá MG -Brasil
andremksh@hotmail.com

**Waldir de Oliveira**
Universidade Federal de Itajubá
Campus Prof. Jose Rodrigues Seabra - Av. BPS nº1303, Bairro Pinheirinho Cep 37500-903 Itajubá MG -Brasil
waldir@unifei.edu.br

***Abstract.*** *The Computational Fluid Dynamics (CFD), is a field of extremely importance in the analysis and design of turbomachines. Techniques of CFD applied to turbomachines have been intensively used in the last decade, resulting in enough realistic models, considering the complex dissipative mechanisms caused by the flow passing between blades. This work intends to show the performance curves of radial fans through a design methodology and analyzes obtained with the integration of source programs and generation of scripts in FORTRAN, so that the programs for generation of geometry and generation of meshes become automatically linked to commercial CFD three-dimensional flow field (FLUENT®), possibilitating the build of the performance curves. The results obtained will be validated with the experimental results.*

***Keywords****: CFD, characteristic curves, turbomachinery, turbulence, fans.*

## 1. INTRODUCTION

CFD has gone a long way since the early development years of the 1960's and today is indispensable part of any design and development stage in all sectors of industry particularly in the area of the flow in internal channels of turbomachines.

Considerable progress has been achieved on the algorithmic side and the computer hardware performance has increased by a significant factor, in terms of both speed and memory. Over the last 30 years computing power has increased by more than a factor of $10^6$, while gains in algorithmic performance can be estimated as close to $10^3$. As a result, full Navier-Stokes codes, with 3D turbulent model, has been applied in up to 20 blade rows and many millions of points (Hirsch and Demeulenaere 2003).

It has been reported many works to validate the complex flow field that occurs in the turbomachines. Notice that a precise representation of the flow field still is in an initial stage. For a complete representation of the many energy dissipation on the flow, it would by necessary mesh mechanisms very refined and transport equations more refined that can capture the secondary flows, vorticity field on the tip and on the hub of the blade, among others. This kinds of works were reported by Anderson et. al. (2003), that studies the validation of many turbomachines which many helpful results were reported that intensifies the use of CFD in the project and analysis of the flow in turbomachines.

Another important aspect is to define the turbulence model appropriately. The influence of specific turbulence model formulation on turbomachinery applications differs substantially for different types of machines. However, almost all machine types found situations where the formulation and proper application of the turbulence model was a key factor in the accurate prediction of the machine characteristic.

As can be observed, full Navier Stokes flow solvers are actually more utilized because they represent physical problems in a more accurate way. In the other hand, it is necessary to engage very powerful computers with very fast execution time to obtain results with high accuracy and reduced time.

In the present work the obtained characteristics of radial fan are analyzed and compared. Pressure coefficient simulated by CFD code (Fluent 6.1®) were compared with experimental results of Oliveira work (2001), obtained in the Federal University Itajubá. Quantitative as well as qualitative conclusions are presented, emphasizing the difficulties to numerically represent the complex flow field in the blades channel of a radial turbomachine.

It is important to highlight that the rotor model geometry is not identicial with the rotor of the experimental analyses, however the principal dimentions are respected.

## 2. EXPERIMENTAL ANALYSIS OF RADIAL FAN:

For the experimental analysis of Oliveira (2001), five centrifugal impellers with different shapes and blade numbers were manufactured. Also a special test rig was build for tests of the centrifugal impeller without irregular external interference in their flow. For determination of the flow characteristics two types of measurement systems were used: one, with an aerodynamic probe located in the centrifugal impeller outlet and, the other, with a load cell for measuring the impeller brake power. A comparison of the results obtained by these two measuring systems shows some important characteristics, such as the phenomenon of the flow recirculation in the centrifugal impeller.

For the experimental analysis, was used $n_{qa}$=150 (n=3000 rpm) as the specific rotation. All the impellers have the same meridian section, as well as the same constructive angles in the inlet and outlet of the blade, differing only in the number of blades and in the format of the transversal section of the blades.

The test rig of centrifugal impeller is shown in Fig (1), with the main components:

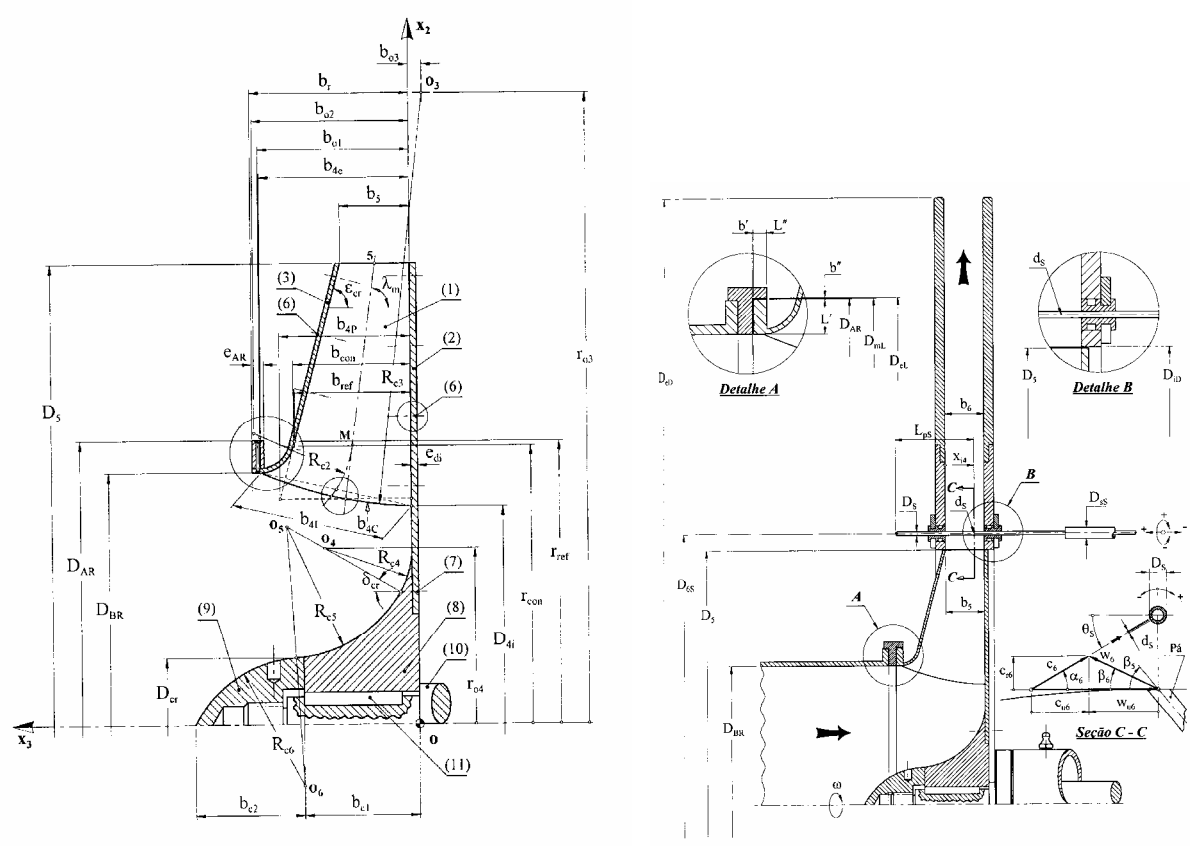


(a) (b)

Figure 1. Scheme of the section of tests ring of the centrifugal impeller.

In figures 1a, and 1b, are shown the meridian section with main dimensions, meridian sections with the Pitot probe position and the transversal section, respectively.

The Pitot probe with two supporting points, was used at the distance $D_{6s}$, in the diffuser section, for the determination of the 3 parameters: flow angle, total and static pressures, based on the non-linear parameter estimation technique (Beck and Arnold, 1977). Other test rig construction details can be found in Oliveira (2001).

Tables 1, 2 e 3 show the main dimensions indicated in the figures.

Table 1. Main meridional section dimensions for the centrifugal impellers with $n_{qa}$=150 end ARC blade profiles (figure 1a and 1b)

| Lengths mm | | Lengths mm | | Lengths mm | | Lengths mm | | Lengths mm | |
|---|---|---|---|---|---|---|---|---|---|
| $b_{4C}$ | 71,141 | $b_{o3}$ | -6,166 | $D_{BR}$ | 229,0 | $r_{ef}$ | 128,5 | $\delta_{cr}$ | 30,0 |
| $b_{4e}$ | 69,0 | $b_{ref}$ | 53,45 | $D_{cr}$ | 60,23 | $R_{c1}$ | 16,0 | $\varepsilon_{cr}$ | 75,277 |
| $b_{4I}$ | 70,721 | $b_r$ | 73,0 | $e_{ar}$ | 5,5 | $R_{c2}$ | 45,491 | $\lambda_m$ | 82,515 |
| $b_{4P}$ | 60,302 | $D_{4C}$ | 207,647 | $e_{de}$ | 2,0 | $R_{c3}$ | 188,802 | | |
| $b_5$ | 32,1 | $D_{4e}$ | 229,014 | $e_{di}$ | 3,0 | $R_{c4}$ | 40,0 | | |
| $b_{cl}$ | 53,0 | $D_{4i}$ | 198,0 | $r_{con}$ | 126,434 | $R_{c5}$ | 60,0 | | |
| $b_{c2}$ | 50,0 | $D_{4I}$ | 213,507 | $r_{o1}$ | 130,5 | $R_{c6}$ | 56,44 | | |
| $b_{com}$ | 53,993 | $D_{4P}$ | 204,85 | $r_{o2}$ | 132,36 | | | | |
| $b_{o1}$ | 69,468 | $D_5$ | 419,5 | $r_{o3}$ | 287,702 | | | | |
| $b_{o2}$ | 72,099 | $D_{AR}$ | 257,5 | $r_{o4}$ | 80,0 | | | | |

Table 2. Main dimensions for the rotor with $n_{qa}$=150 (figure 1.b)

| Lengths mm | | Lengths mm | | Lengths mm | | Lengths Mm | | Lengths Mm | |
|---|---|---|---|---|---|---|---|---|---|
| $b_5$ | 32,1 | $D_{AR}$ | 257,5 | $D_{iL}$ | 420,5 | L’ | 14,25 | $X_{14}$ | 2,236 |
| $b_6$ | 32,2 | $D_{BR}$ | 229,0 | $D_{mL}$ | 258,0 | L” | 5,5 | $x_{24}$ | 10,626 |
| b’ | 0,5 | $D_{6S}$ | 447,0 | $d_S$ | 0,35 | $L_B$ | 237,0 | $x_{34}$ | 21,574 |
| b” | 0,5 | $D_{eD}$ | 1000,0 | $D_S$ | 3,0 | $L_{pS}$ | 65,0 | $x_{44}$ | 29,964 |
| $D_5$ | 419,5 | $D_{eL}$ | 258,5 | $D_{sS}$ | 9,5 | $s_{RC}$ | 170,0 | | |

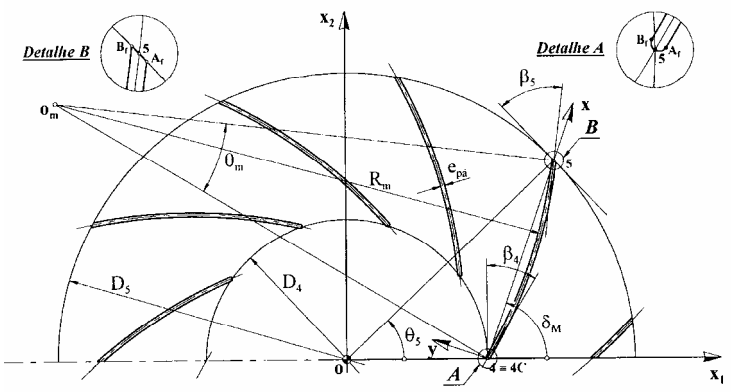


Figure 3. Partial sketch of the transversal section of the centrifugal rotor with $n_{qa}$=150, with ARC blades

Table 3. Main dimensions of the transversal section of the centrifugal rotor with $n_{qa}$=150, with ARC blades

| Lengths mm | | Lengths mm | | Angles ° | | Angles ° | | Angles ° | |
|---|---|---|---|---|---|---|---|---|---|
| $D_{4C}$ | 207,647 | $\ell$ | 150,171 | $\beta_{4C}$ | 31,87 | $\lambda_C$ | 31,634 | $\theta_{5p}$ | 41,749 |
| $D_{4I}$ | 213,507 | $r_{4C}$ | 104,621 | $\beta_{4I}$ | 33,50 | $\theta_{4c}$ | 0,699 | $\theta_{5s}$ | 42,812 |
| $D_{4P}$ | 204,85 | $r_{4p}$ | 105,891 | $\beta_{4P}$ | 31,02 | $\theta_{4p}$ | 0,265 | $\theta_m$ | 23,700 |
| $D_5$ | 419,5 | $r_{4s}$ | 103,356 | $\beta_5$ | 50,41 | $\theta_{4s}$ | 1,143 | $\theta_p$ | 23,311 |
| $e_{pá}$ | 3,0 | $R_m$ | 365,013 | $\delta_M$ | 70,00 | $\theta_5$ | 42,282 | $\theta_s$ | 23,742 |

## 3. CFD APLIED TO TURBOMACHINES – CONCEPTUAL MODEL

In this work, the Fluent® (2003) software was used to calculate the flow in the channel of the centrifugal fan. For automatic geometry and mesh generation of the impeller, a data file in Fortran was used as a script to read this data file with the software ANSYS ICEM CFD®. This technique allows the fast obtain of the main impeller's dimension from the pressure and the flow mass from the project's data.

The mesh chosen was the HEXA type, because it shows the most stability in the result convergence. The differential equations below describe the flow field on a non-inertial system, more details can be found in Vavra (1974) and Wu (1952).

In this work the technique of Rotating Reference Frame RRF is used. This methodology is applied to impellers in mixing tanks, rotating turbomachinery blades (centrifugal impellers, axial fans, etc.), flows in rotating passages (e.g., cooling ducts, secondary air circuits, and disk cavities in rotating equipment).

When such problems are defined in a rotating reference frame, the rotating boundaries become stationary relative to the rotating frame, since they are moving at the same speed as the reference frame.

The Equations for a Rotating Reference Frame are solved in a rotating frame of reference. The acceleration of the fluid that appear in the momentum equations is augmented by additional acceleration terms. The governing equations for the analyses of fluid flow in the channel of the turbomachine are:

-The mass conservation equation for 2D axisymmetric geometries (continuity) is given by:

$$\frac{\partial \rho}{\partial t} + \frac{\partial (\rho v_x)}{\partial x} + \frac{\partial (\rho v_r)}{\partial r} + \frac{\rho v_r}{r} = 0 \tag{1}$$

where $x$ is the axial coordinate, $r$ is the radial coordinate, $v_x$ is the axial velocity, and $v_r$ is the radial velocity.

-Momentum Conservation Equations in an inertial (non-accelerating) reference frame, is described in the following way:

$$\frac{\partial}{\partial t}(\rho \vec{v}) + \nabla \cdot (\rho \vec{v} \vec{v}) = -\nabla p + \nabla \cdot (\bar{\bar{\tau}}) + \rho \vec{g} + \vec{F} \,, \tag{2}$$

where $p$ is the static pressure, $\bar{\bar{\tau}}$ is the stress tensor (described below), and $\rho \vec{g}$ and $\vec{F}$ are the gravitational body force and external body forces (e.g., that arise from interaction with the dispersed phase), respectively. $\vec{F}$ also contains other model-dependent source terms such as porous-media and user-defined sources.

The stress tensor $\bar{\bar{\tau}}$ is given by:

$$\bar{\bar{\tau}} = \mu \left[ \left( \nabla \vec{v} + \nabla \vec{v}^T \right) - \frac{2}{3} \nabla \cdot \vec{v} I \right], \tag{3}$$

where $\mu$ is the molecular viscosity, $I$ is the unit tensor, and the second term on the right hand side is the effect of volume dilation.

For 2D axisymmetric geometries, the axial and radial momentum conservation equations are given by:

$$\frac{\partial}{\partial t}(\rho \vec{v}_x) + \frac{1}{r}\frac{\partial}{\partial x}(r \rho v_x v_x) + \frac{1}{r}\frac{\partial}{\partial r}(r \rho v_r v_x) = -\frac{\partial p}{\partial x} + \frac{1}{r}\frac{\partial}{\partial x}\left[ r\mu \left( 2\frac{\partial v_x}{\partial x} - \frac{2}{3}(\nabla \cdot \vec{v}) \right) \right] + \frac{1}{r}\frac{\partial}{\partial r}\left[ r\mu \left( 2\frac{\partial v_x}{\partial r} - \frac{\partial v_r}{\partial x} \right) \right] + F_x \tag{4}$$

$$\frac{\partial}{\partial t}(\rho \vec{v}_r) + \frac{1}{r}\frac{\partial}{\partial x}(r \rho v_x v_r) + \frac{1}{r}\frac{\partial}{\partial r}(r \rho v_r v_r) = -\frac{\partial p}{\partial r} + \frac{1}{r}\frac{\partial}{\partial x}\left[ r\mu \left( 2\frac{\partial v_r}{\partial x} + \frac{\partial v_x}{\partial r} \right) \right] + \frac{1}{r}\frac{\partial}{\partial r}\left[ r\mu \left( 2\frac{\partial v_r}{\partial r} - \frac{2}{3}(\nabla \cdot \vec{v}) \right) \right] - 2\mu \frac{v_r}{r^2} + \frac{2}{3}\frac{\mu}{r}(\nabla \cdot \vec{v}) + \rho \frac{v_z^2}{r} + F_r \tag{5}$$

where, $\nabla \cdot \vec{v} = \frac{\partial v_x}{\partial x} + \frac{\partial v_r}{\partial r} + \frac{v_r}{r}$

and $v_z$ is the swirl velocity.

When the equations of motion, Eq. (4) and (5), are solved in a rotating frame of reference, the acceleration of the fluid is augmented by additional terms. The model allows a solution using either the absolute velocity, $\vec{v}$, or relative velocity, $\vec{v}_r$, as the dependent variable. The two velocities are related by the following equation:

$$\vec{v}_r = \vec{v} - (\vec{\Omega} \times \vec{r}) \tag{6}$$

Here, $\vec{\Omega}$ is the angular velocity vector (that is, the angular velocity of the rotating frame) and $\vec{r}$ is the position vector in the rotating frame.
The left-hand side of the momentum equations Eq. (2) appears as follows for an inertial reference frame:

$$\frac{\partial}{\partial t}(\rho\vec{v}) + \nabla \cdot (\rho\vec{v}_r\vec{v}) + \rho(\vec{\Omega} \times \vec{v}) \tag{7}$$

In terms of relative velocities the left-hand side is given by

$$\frac{\partial}{\partial t}(\rho\vec{v}_r) + \nabla \cdot (\rho\vec{v}_r\vec{v}_r) + \rho(2\vec{\Omega} \times \vec{v}_r + \vec{\Omega} \times \vec{\Omega} \times \vec{r}) + \rho\frac{\partial\vec{\Omega}}{\partial t} \times \vec{r} \tag{8}$$

Where $\rho(2\vec{\Omega} \times \vec{v}_r)$ is the Coriolis force. Note that in the equation there is the term $\rho\frac{\partial\vec{\Omega}}{\partial t} \times \vec{r}$, so it cannot accurately model a time-varing angular velocity using the relative velocity formulation.

For flows in rotating domains, the equation for conservation of mass, or continuity equation, can be written as follows for both the absolute and the relative velocity formulation, Vavra (1974).

In this work for turbulence models it was used the standard *k*-ε model, which is a semi-empirical model based on the transport equations for the turbulent kinetic energy (*k*) and its dissipation rate (ε). The model transport equation for *k* is derived from the exact equation, while the model transport equation for ε is obtained using physical reasoning and bears little resemblance to its mathematically exact counterpart.

In the derivation of the *k*-ε model, it was assumed that the flow is fully turbulent, and the effects of molecular viscosity are negligible. The standard *k*-ε model is therefore valid only for fully turbulent flows. The turbulent kinetic energy, *k*, and its rate of dissipation, ε, are obtained from the following transport equations:

$$\rho\frac{Dk}{Dt} = \frac{\partial}{\partial x_i}\left[\left(\mu + \frac{\mu_t}{\sigma_k}\right)\frac{\partial k}{\partial x_i}\right] + G_k + G_b - \rho\varepsilon - Y_M \tag{9}$$

and

$$\rho\frac{D\varepsilon}{Dt} = \frac{\partial}{\partial x_i}\left[\left(\mu + \frac{\mu_t}{\sigma_\varepsilon}\right)\frac{\partial \varepsilon}{\partial x_i}\right] + G_{1\varepsilon}\frac{\varepsilon}{k}(G_k + C_{3\varepsilon}G_b) - C_{2\varepsilon}\rho\frac{\varepsilon^2}{k} \tag{10}$$

In these equations, $G_k$ represents the generation of turbulent kinetic energy due to the mean velocity gradients, $G_b$ is the generation of turbulent kinetic energy due to buoyancy. $Y_M$ represents the contribution of the fluctuating dilatation in compressible turbulence to the overall dissipation rate, calculated as described . $C_{1\varepsilon}$, $C_{2\varepsilon}$, and $C_{3\varepsilon}$ are constants. $\sigma_k$ and $\sigma_\varepsilon$ are the turbulent Prandtl numbers for *k* and *ε*, respectively.

The turbulent viscosity, $\mu_t$, is computed by combining *k* and ε as follows:

$$\mu_t = \rho C_\mu \frac{k^2}{\varepsilon} \tag{11}$$

where $C_\mu$ is a constant.
The model constants are defined as: $C_{1\varepsilon}$,=1.44, $C_{2\varepsilon}$ =1.92, $C_\mu$,=0.09 $\sigma_k$ =1.0 and $\sigma_\varepsilon$ =1.3.

These default values have been determined experimentally with air and water for fundamental turbulent shear flows including homogeneous shear flows and decaying isotropic grid turbulence. They have been found to work fairly well for a wide range of wall-bounded and free shear flows. Other details of the formulation can be found in Wilcox (1998), Versteeg et al ( 1995).

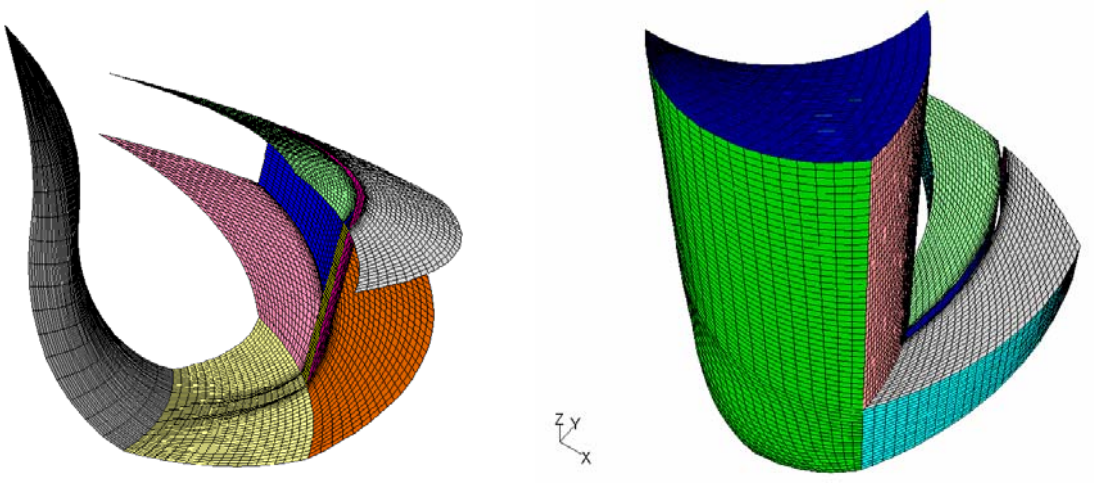


Figure 4. Grid with 85956 cells and 263969 faces

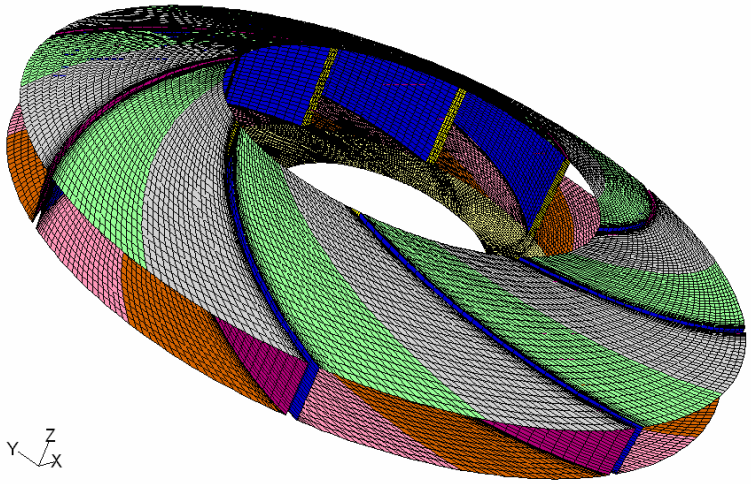


Figure 5. Periodic repeat view with 8 blades

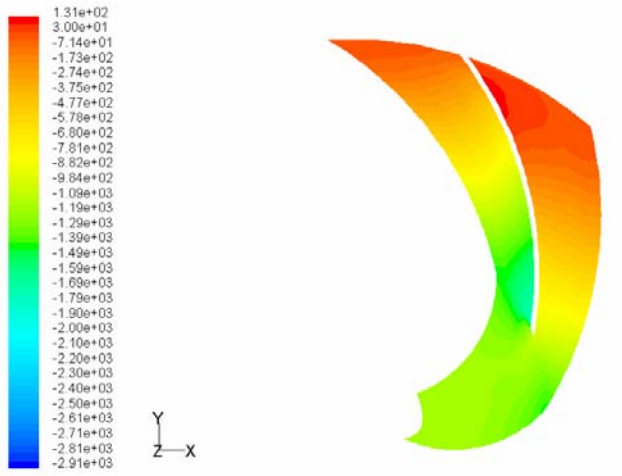


Figure 6. Contours of static pressure (Pascal) for $\psi = 0.69433$ – Transversal plane view at 50 % of height

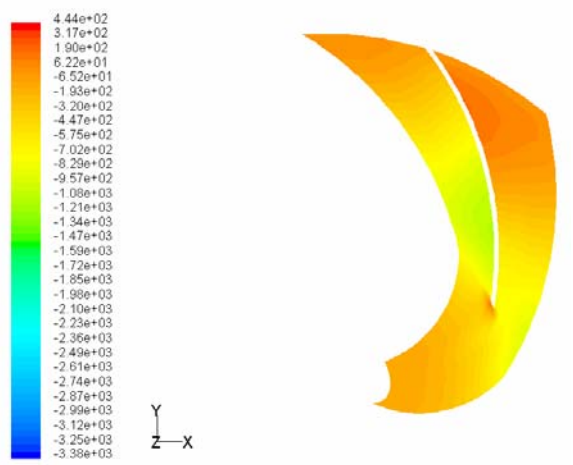


Figure 7. Contours of static pressure (Pascal) for ψ = 0.62914 – Transversal plane view at 50% of height

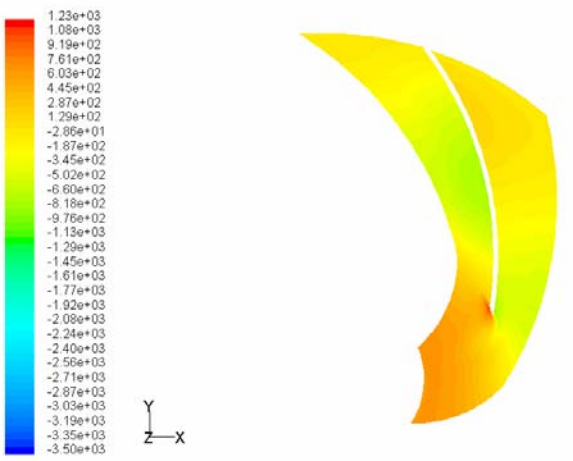


Figure 8. Contours of static pressure (Pascal) for ψ = 0.53377 – Transversal plane view at 50% of height

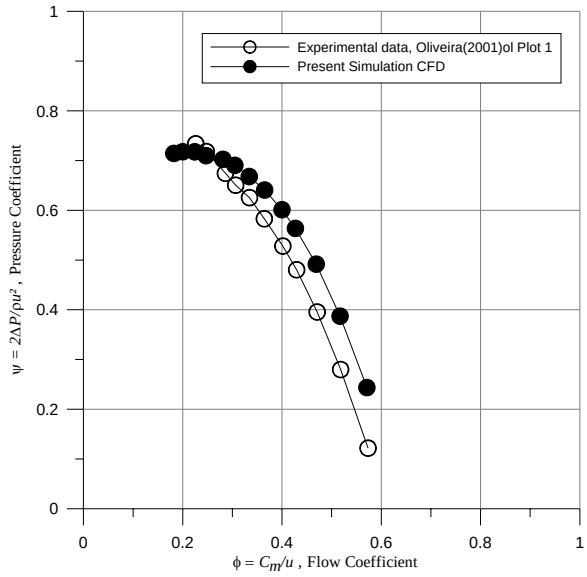


Figure 9. Pressure and flow coefficient for radial impeller, $n_{qa}$=150

## 4. RESULTS

Figures 6, 7 e 8 represent the static pressure file in the transversal section of the rotor channel at 50% width of the blade, where it can be observed the static pressure recuperation due to mass flow increase.

Other flow field representations can be determined, eg., absolute and relative velocity fields, regions of separation of the boundary layer, recirculation, secondary flows and turbulence field. Nevertheless, it is of most importance the determination of global variables that represent the machine operation characteristics. In the other hand, to obtain trustful representations of the flow kinetics it is required refined meshes and more restricted convergence criteria, what requires more efficient computer processors.

For the validation of the numerical simulation using Fluent 6.1 software, the coefficients $\psi$ (pressure) and $\phi$ (flow) were compared for the rotor with 8 ARC blades (Fig. 9) at 3000 rpm. The pressure coefficient is defined by $\psi = 2\Delta P / \rho U^2$, where $\Delta P$ is the difference between the total pressure at rotor inlet and outlet, $U_5$ the tangential or peripheral velocity at the diameter $D_5$ and $\rho$ is the air specific mass.

It must be noted that for that dynamic pressure calculation the relative flow must be used instead of the absolute one.

Regarding the boundary conditions, periodicity, wall, inlet and outlet conditions were set. For inlet conditions the mass flow was obtained from the flow coefficient calculated from experiments.

Although the shape of the curve obtained from numerical simulation (Fig. 9) agree in a wide range of operation, they meet at low mass flows, what may be attributed to the fact that the machines are not exactly the same: the machine rotor the blade leading edge is rounded, decreasing the incidence loss, while the computational model is not.

According to Oberkampf and Trucano (2002) the differences between CFD calculations and actual measurements are due to four error sources $E_\Delta = E_1 + E_2 + E_3 + E_4$, where: $E_1$ is due to the measurement (difference between the value of the current and the experimentally obtained, $E_1 = \phi_{real} - \phi_{experimental}$. $E_2$ is the model errors due to the considerations made for the conceptual model. It is the difference between the experimental value and the one that would be obtained in the exact solution of the equations of the model experiment, $E_2 = \phi_{experimental} - \phi_{exato.}$ $E_3$ is the error related to the numerical schemes, due to the difference between the exact solution value and the one that would be numerically calculated by and ideal computer capable of infinite spacial and time refinement, that is, infinite precision, $E_3 = \phi_{exato} - \phi_{ideal}$. Finally, $E_4$ is the error due to the limitations of numerical calculation. It is the difference between the results from an ideal and a real computer, obtained by simulation, $E_4 = \phi_{ideal} - \phi_{simulation}$.

## 5. CONCLUSIONS

It has been possible to validate quantitatively the characteristic curve of a centrifugal fan with 8 blades, rotating at n=3000 rpm and specific speed $n_{qa}$=150. The results obtained by numerical simulation agree well with the experimental results.

It is important to mention that the better results would be obtained provided that better and refined meshes were used, what requires more computational effort.

Based on the results of this work, it is possible to use the same methodology for the study of other types of turbomachines, like axial fans, compressors, turbines and pumps.

## 6. REFERENCES


Anderson, M.R., Gu, Fahua, MacLeod, P.D, 2003, "Application and Validation of CFD in Turbomachinery Design System", ASME International Mechanical Engineering Congress and R&D Expo, Washington, D.C.

Beck, J.V., Arnold, K.J., 1977, "Parameter estimation in engineering and science", New York : John Wiley and Sons. 501p.

Fluent Inc, 2003. Fluent 6.1 User's Guide. [S.I]

Hirsch, C., Demeulenaere, A., 2003 "State of the Art in the Industrial CFD for Turbomachinery Flows" QNET-CFD Network Newsletter, Volume 2, No. 3.

Oberkampf, W.L. and Trucano, T.G., 2000, "Validation Methodology in Computational Fluid Dynamics" AIAA Paper 2000-2549 p.

Oliveira, W., 2001, "Analise do Escoamento em Turbomáquinas Radiais", Tese de Doutorado, Instituto Tecnológico de Aeronáutica, ITA, 236p.

Wilcox, D. C., 1998, "Turbulence Modeling for CFD". DCW Industries, Inc.

Wu, C.H., 1952 " A General Theory of Three-Dimesional Flow in Subsonic and Supersonic Turbomachines of Axial – Radial – and Mixed Flow Types", NACA TN 2604.

Versteeg, H. K. and Malalasekera, W., 1995, 'An Introduction to Computational Fluid Dynamics: The Finite Volume Method". Addison Wesley Longman, Ltd., Harlow, England.